

Article

First-Principles Study of the Nonlinear Elasticity of Rare-Earth Hexaborides REB_6 ($RE = La, Ce$)

Xianshi Zeng^{1,2}, Yuanxiu Ye¹, Shenlin Zou¹, Qingdong Gou¹, Yufeng Wen^{1,3,*} and Ping Ou^{3,4}

¹ School of Mathematical Sciences and Physics, Jinggangshan University, Ji'an 343009, China; zengxueliang@163.com (X.Z.); jgsxy_yyx@sohu.com (Y.Y.); shenlinz@sina.com (S.Z.); gouqingdong@163.com (Q.G.)

² Research Center of Laser Fusion, China Academy of Engineering Physics, Mianyang 621900, China

³ School of Materials Science and Engineering, Shanghai Jiaotong University, Shanghai 200240, China; opyp@163.com

⁴ School of Materials Science and Engineering, Jiangxi University of Science and Technology, Ganzhou 341000, China

* Correspondence: jgsuwyf@sina.com; Tel.: +86-796-8100-488

Academic Editor: Helmut Cölfen

Received: 30 March 2017; Accepted: 20 October 2017; Published: 25 October 2017

Abstract: The complete set of independent second- and third-order elastic constants of rare-earth hexaborides LaB_6 and CeB_6 are determined by the combination method of first-principles calculations and homogeneous deformation theory. The ground-state lattice parameters, second-order elastic constants, and bulk modulus are in reasonable agreement with the available experimental data. The third-order elastic constant of longitudinal mode C_{111} has a larger absolute value than other shear modes, showing the contribution to lattice vibrations from longitudinal modes to be greater. The pressure derivatives of the second-order elastic constants related to the third-order elastic constants are calculated to be positive for the two hexaborides, which are consistent with those of their polycrystalline bulk modulus and shear modulus. Furthermore, the effect of pressure on the structural stability, mechanical property, and elastic anisotropy of the two hexaborides are investigated, showing a reduction in mechanical stability and an increase in ductility and anisotropy with increasing pressure.

Keywords: rare-earth hexaborides; elastic constants; mechanical property; elastic anisotropy; first-principles

1. Introduction

Rare-earth hexaborides (REB_6) have been widely used in various field-electron emitter devices and high-energy optical systems due to their attractive properties of high melting point, high mechanical strength, low work function, low volatility at high temperatures, conductivity, chemical resistance, brightness, small optical size, long service life, and the monoenergetic character of their electrons [1]. These attractive properties are closely related to their crystal structure, which is a simple cubic CsCl (space group $Pm\bar{3}m$) structure with boron octahedra at the cube corners and a rare-earth atom occupying the body-center position. In this structure, each rare-earth atom is surrounded by eight boron octahedra, and the boron octahedra are linked together into a three-dimensional network. It is generally accepted that the structural peculiarity should be taken as one of the basic starting points to explain some of the anomalies in the REB_6 systems. Currently, research focuses on the developments and applications of the REB_6 nanostructures. Understanding the mechanical behavior of these structures is very important in the development and application stages. It is well-known that nonlinear effects become significant in nanostructural materials. Nonlinear elastic properties are

important for describing nonlinear effects in mechanical behavior. Thus, it is very necessary to study nonlinear effects in the elasticity of the hexaborides.

In general, the second-order elastic constants (SOECs) C_{ij} describe the linear elastic stress–strain response for single crystals. Third-order elastic constants (TOECs) C_{ijk} are important quantities to characterize the nonlinear elasticity of the crystals. Both SOECs and TOECs are important parameters to model the mechanical response of crystals under high pressure. Tanaka et al. [2] have made measurements of the transit times of pulses of longitudinal and transverse ultrasonic waves propagating in single crystal LaB_6 at room temperature, and have determined its SOECs from the resultant velocities. Baranovskiy et al. [3] measured the sound velocities along the principal crystallographic axes of LaB_6 at 78 K by employing the phase–frequency method, and evaluated its SOECs and bulk modulus from the resultant sound velocities. Nakamura et al. [4,5] performed sound velocity measurements with an ultrasonic apparatus based on the phase comparison method to investigate the temperature dependence of the SOECs in LaB_6 and CeB_6 . Goto et al. [6] also studied the temperature dependence of the SOECs in CeB_6 . Lüthi et al. [7] took the ultrasonic and Brillouin scattering measurements to redetermine the SOECs of CeB_6 at room temperature. Moreover, Gürel and Eryiğit [8] used a first-principles calculations method to study structural, elastic, lattice-dynamical, and thermodynamical properties of LaB_6 and CeB_6 . Tang et al. [9] performed a first-principles study of structural, elastic, and electronic properties of CeB_6 under pressure. Besides, high-pressure phase transitions in LaB_6 and CeB_6 have been investigated experimentally. By using Raman and X-ray diffraction measurements on LaB_6 , Teredesai et al. [10] proposed that a phase transition from cubic to orthorhombic crystal structure occurs around 10 GPa, while Godwal et al. [11] stated that there is no structural phase transitions up to at least 25 GPa. By using X-ray diffraction measurements on CeB_6 , Leger et al. [12] revealed no structural phase transition at ambient temperature up to 20 GPa. Foroozani et al. [13] failed to detect any change in crystal structure up to 85 GPa, but they did not exclude the possibility of structural changes in the pressure range of 85–122 GPa. Nevertheless, the TOECs and related elastic properties of LaB_6 and CeB_6 have not yet been investigated either experimentally or theoretically to the best knowledge of the authors.

In recent years, first-principles calculations based on density functional theory (DFT) have been employed to successfully determine the SOECs, TOECs, and higher-order elastic constants of single crystals by utilizing a series of homogeneous deformation strains applied to a crystalline system to obtain the energy–strain relations [14–16]. To study the nonlinear effects in the elasticity of LaB_6 and CeB_6 , we shall use the same method to determine the SOECs and TOECs of both hexaborides. Subsequently, the pressure derivatives of the effective SOECs have been estimated from the obtained values of SOECs and TOECs. The polycrystalline bulk, shear, and Young’s moduli, Poisson’s ratio, and their pressure dependence in LaB_6 and CeB_6 have also been studied along with the elastic anisotropy of the two hexaborides. The paper is organized as follows. In Section 2, a brief description of computational methodology is given. In Section 3, the results we have obtained are presented with available experimental and theoretical values for comparison. Finally, the conclusions are drawn in Section 4.

2. Computational Methods

2.1. First-Principles Total-Energy Calculations

First-principles calculations have been performed by means of the Vienna Ab initio simulation package (VASP) code based on density functional theory (DFT) [17–19]. The projector augmented wave (PAW) method was used for describing the ion–electron interaction [20,21]. The generalized gradient approximation (GGA) of Perdew–Burke–Ernzerhof (PBE) was used for evaluating the exchange–correlation energy [22,23]. The standard PAW potentials were used for La, Ce, and B elements. A cutoff energy of 600 eV was chosen for the plane wave basis. A threshold of 10^{-6} eV per atom on total energy was set for the convergence of electronic self-consistency. A $15 \times 15 \times 15$

Monkhorst–Pack grid of k -point was adopted for sampling the Brillouin zone [24]. Before calculating the elastic constants, the structures of LaB_6 and CeB_6 were fully relaxed with respect to the volume, shape, and internal atomic position until the atomic forces were less than $0.01 \text{ eV}/\text{\AA}$. To accurately calculate the elastic constants, the linear tetrahedron method was used for the final self-consistent calculations of total-energies.

2.2. SOECs and TOECs of Single Crystal

In this paper, the method of the finite-strain continuum elasticity theory is employed to calculate the SOECs and TOECs. Here we discuss the theory briefly, the details of which have been given in References [25–29]. Let a_i be the initial Cartesian coordinates of a material point in the unstrained state. A finite homogeneous deformation carries the material point to the final position with the coordinates x_i in the strained state. After introducing the Jacobian deformation gradient

$$J_{ij} = \frac{\partial x_i}{\partial a_j} (i, j = 1, 2, 3), \quad (1)$$

the Lagrangian strain tensor in the stressed state may be defined as

$$\eta_{ij} = \frac{1}{2} \sum_{r=1}^3 (J_{ri} J_{rj} - \delta_{ij}). \quad (2)$$

The elastic strain energy (ΔE) can be expanded in a Taylor series in terms of the strain tensor as

$$\Delta E = \frac{V}{2!} \sum_{ijkl} C_{ijkl} \eta_{ij} \eta_{kl} + \frac{V}{3!} \sum_{ijklmn} C_{ijklmn} \eta_{ij} \eta_{kl} \eta_{mn} + O(\eta^4), \quad (3)$$

where V is the volume of the unstrained lattice. After applying the Voigt notation ($11 \rightarrow 1, 22 \rightarrow 2, 33 \rightarrow 3, 23 \rightarrow 4, 13 \rightarrow 5, \text{ and } 12 \rightarrow 6$) to denote the strain tensor, the strain energy can be rewritten as

$$\Delta E = \frac{V}{2!} \sum_{ij} C_{ij} \eta_i \eta_j + \frac{V}{3!} \sum_{ijk} C_{ijk} \eta_i \eta_j \eta_k + O(\eta^4). \quad (4)$$

For cubic systems, there are three independent SOECs (C_{11}, C_{12}, C_{44}) and six dependent TOECs ($C_{111}, C_{112}, C_{123}, C_{144}, C_{155}, C_{456}$). To obtain the complete set of SOECs and TOECs of LaB_6 and CeB_6 , we used six Lagrangian strain tensors in terms of a single strain parameter ζ . Table 1 gives the relationship between the coefficients A_2 and A_3 and SOECs and TOECs for the six selected strain tensors. For each strain tensor, the strain parameter ζ varied from -0.08 to 0.08 in steps of 0.01 . Inserting these strain tensors into Equation (4), the strain energy density Φ can be written as an expansion in the strain parameter ζ as

$$\Phi = \frac{\Delta E}{V} = \frac{1}{2} A_2 \zeta^2 + \frac{1}{6} A_3 \zeta^3 + O(\zeta^4), \quad (5)$$

where A_2 and A_3 are the combinations of SOECs and TOECs, respectively. For every deformed configuration, the atomic positions were optimized, and the total-energy was calculated by using first-principles method based on DFT. The strain energy is defined as the total-energy difference between the deformed and the perfect crystals. In this way, the dependencies of the strain energy ΔE on the strain parameter ζ were obtained for each homogeneous deformation. By comparing with the expressions from the finite-strain elasticity theory given in Table 1, the elastic constants were extracted from a polynomial fit to the strain energy versus strain parameter curves under the various strains.

Table 1. The coefficients A_2 and A_3 in Equation (5) of the corresponding selected strain tensors as the linear combinations of the second- and third-order elastic constants for cubic crystal [14].

Strain	A_2	A_3
$\eta_1 = (\xi, 0, 0, 0, 0, 0)$	C_{11}	C_{111}
$\eta_2 = (\xi, \xi, 0, 0, 0, 0)$	$2C_{11} + 2C_{12}$	$2C_{111} + 6C_{112}$
$\eta_3 = (\xi, \xi, \xi, 0, 0, 0)$	$3C_{11} + 6C_{12}$	$3C_{111} + 18C_{112} + 6C_{123}$
$\eta_4 = (\xi, 0, 0, 2\xi, 0, 0)$	$C_{11} + 4C_{44}$	$C_{111} + 12C_{144}$
$\eta_5 = (\xi, 0, 0, 0, 2\xi, 0)$	$C_{11} + 4C_{44}$	$C_{111} + 12C_{155}$
$\eta_6 = (0, 0, 0, 2\xi, 2\xi, 2\xi)$	$12C_{44}$	$48C_{456}$

2.3. Pressure Derivatives of the Effective SOECs

When an external hydrostatic pressure is applied to a crystal, the effective SOECs are very useful to describe the nonlinear elastic properties of the crystal. Usually, the effective SOECs under hydrostatic pressure P ($C_{ij}(P)$) can be expanded by a Taylor expansion as [15]

$$C_{ij}(P) \approx C_{ij} + \frac{dC_{ij}(P)}{dP}P = C_{ij} + C'_{ij}P, \quad (6)$$

where C'_{ij} is the first-order pressure derivative, which can be determined from SOECs and TOECs, and can be expressed for cubic systems as [15,25]

$$\begin{aligned} C'_{11} &= -\frac{C_{111} + 2C_{112} + 2C_{11} + 2C_{12}}{C_{11} + 2C_{12}}, \\ C'_{12} &= -\frac{2C_{112} + C_{123} - C_{11} - C_{12}}{C_{11} + 2C_{12}}, \\ C'_{44} &= -\frac{2C_{155} + C_{144} + C_{11} + 2C_{12} + C_{44}}{C_{11} + 2C_{12}}. \end{aligned} \quad (7)$$

2.4. Pressure Derivatives of Polycrystalline Elastic Moduli

On the basis of the effective elastic constants, the bulk modulus B and shear modulus G for LaB_6 and CeB_6 under different pressure were obtained using the Voigt, Reuss, and Hill approximations [30–32]. For the specific case of cubic structures, the Voigt's and Reuss's bulk moduli can be expressed as

$$B_V = B_R = \frac{C_{11} + 2C_{12}}{3}, \quad (8)$$

and the Voigt's and Reuss's shear moduli are defined as

$$\begin{aligned} G_V &= \frac{C_{11} - C_{12} + 3C_{44}}{5}, \\ G_R &= \frac{5(C_{11} - C_{12})C_{44}}{3(C_{11} - C_{12}) + 4C_{44}}. \end{aligned} \quad (9)$$

Hill proposed that the effective elastic moduli are the arithmetic averages of the Voigt and Reuss moduli, and thus obtained by

$$\begin{aligned} B_H &= \frac{B_V + B_R}{2}, \\ G_H &= \frac{G_V + G_R}{2}, \end{aligned} \quad (10)$$

where the subscripts "V" and "R" correspond to the Voigt and Reuss bounds, and the subscript "H" represents the Hill averaging method. The Young's modulus (E) and Poisson's ratio (ν) are given by

$$E_X = \frac{9B_X G_X}{3B_X + G_X},$$

$$\nu_X = \frac{3B_X - 2G_X}{2(3B_X + G_X)},$$
(11)

where $X = V, R, H$. The pressure derivative of the bulk and shear moduli can be given by

$$B'_H = B'_V = B'_R = \frac{C'_{11} + 2C'_{12}}{3},$$

$$G'_V = \frac{C'_{11} - C'_{12} + 3C'_{44}}{5},$$

$$G'_R = \frac{5[3(C_{11} - C_{12})^2 C'_{44} + 4(C'_{11} - C'_{12})C_{44}^2]}{[3(C_{11} - C_{12}) + 4C_{44}]^2},$$

$$G'_H = \frac{G'_V + G'_R}{2}.$$
(12)

The pressure derivative of the Young's modulus E'_X and the Poisson's ratio ν'_X can be given by

$$E'_X = \frac{9(3B_X^2 G'_X + B'_X G_X^2)}{(3B_X + G_X)^2},$$

$$\nu'_X = \frac{9(B'_X G_X - B_X G'_X)}{2(3B_X + G_X)^2}.$$
(13)

Under the external hydrostatic pressure P , the polycrystalline elastic moduli $Y_X(P)$ ($Y = B, G, E, \nu$) can be given by

$$Y_X(P) = Y_X + \frac{dY_X(P)}{dP} P = Y_X + Y'_X P.$$
(14)

3. Results and Discussion

3.1. Second-Order and Third-Order Elastic Constants of REB_6 ($RE = La, Ce$)

The calculated results of the lattice parameters and the SOECs of LaB_6 and CeB_6 at ground-state are listed in Table 2 along with the published experimental values and other calculated results [2–9,13,33,34]. Comparison of the lattice constants shows that the calculated quantities of the present work are in excellent agreement with the previous experimental and theoretical values. The maximum relative error between our calculated result and the experimental data is 0.07% (0.65%) for LaB_6 (CeB_6), and that between our and other calculated results correspond to 0.63% (0.96%) for LaB_6 (CeB_6). The room-temperature lattice constant of LaB_6 was measured as 4.156 Å from the X-ray power diffraction patterns [2], which is larger than that (4.1407 Å) of CeB_6 [34]. It is the same with the results obtained in this study. These can be explained well by the larger atomic radius of La (2.74 Å) compared with Ce (2.70 Å) [35].

The strain energy versus strain parameter curves under the various strains are fitted with a suitable polynomial to obtain the coefficients A_2 and A_3 in the Equation (5) for determining the SOECs and TOECs, as illustrated in Figure 1. The discrete points and the solid lines represent the results obtained from the first principles calculations and fitted polynomials, respectively. Obviously, these dependent curves of the strain energy on the strain have the characteristics of the asymmetry, which is the expected behavior under finite-strain elastic deformation. The strain energy with negative strains is always larger than that with positive strains, and thus the TOECs are typically negative. The fitted curves match well with the first-principles calculations results. For the values of SOECs, it is possible that some constants may be determined from a few polynomial fits (e.g., C_{44} from coefficients in $f_4(\eta)$, $f_5(\eta)$, and $f_6(\eta)$), together with obtaining slightly different results (e.g., for LaB_6 , $C_{44} = 90.2, 89.1$, and 91.0 GPa from $f_4(\eta)$, $f_5(\eta)$, and $f_6(\eta)$). In such cases, the average value of all results is given in

Table 2. Measurements of the SOECs for LaB₆ and CeB₆ exhibit large discrepancies among themselves, partly because of different techniques to obtain them. Especially, the SOEC C_{12} of CeB₆ was measured to be large negative in reference [6] while positive in references [5,7]. For LaB₆, the calculated SOECs of the present study are in reasonable accordance with the previous experimental and theoretical results [2–4,8]. For CeB₆, a negative value of C_{12} reported in reference [6] was also not found in the present study. The calculated results of the SOECs are also in reasonable agreement with other experiments [5,7] and previous calculations [8,9]. For the two hexaborides, the SOEC C_{11} measures the resistance to linear compression along the uniaxial axes, and the others are mainly related to the non-axial sound propagation. The values of C_{11} are significantly larger than the others in both systems, implying that they are difficult to compress under uniaxial stress. In addition, the ground-state SOECs of LaB₆ and CeB₆ can satisfy the three Born stability criteria for the cubic system [36]: $C_{11} + 2C_{12} > 0$, $C_{11} - C_{12} > 0$ and $C_{44} > 0$, and thus their cubic structures are both mechanically stable.

Table 2. Lattice parameter a (in Å) and elastic constants C_{ij} (in GPa) of LaB₆ and CeB₆.

Crystal	Method	a	C_{11}	C_{12}	C_{44}
LaB ₆	Present	4.154	474.1	24.3	90.1
	Exp. [2]	4.156	453.3	18.2	90.1
	Exp. [4,33]	4.1569	478	43	84
	Exp. [3]	4.1565	463	45	89
	The. [8]	4.1277	466	37	88
CeB ₆	Present	4.114	488.2	17.9	74.8
	Exp. [5,13]	4.132	473	16	81
	Exp. [7,34]	4.1407	508	19	79
	Exp. [7]		472	53	78
	Exp. [6]		406	−93	78
	The. [9]	4.121	483	10	75
	The. [8]	4.154	452	34	98

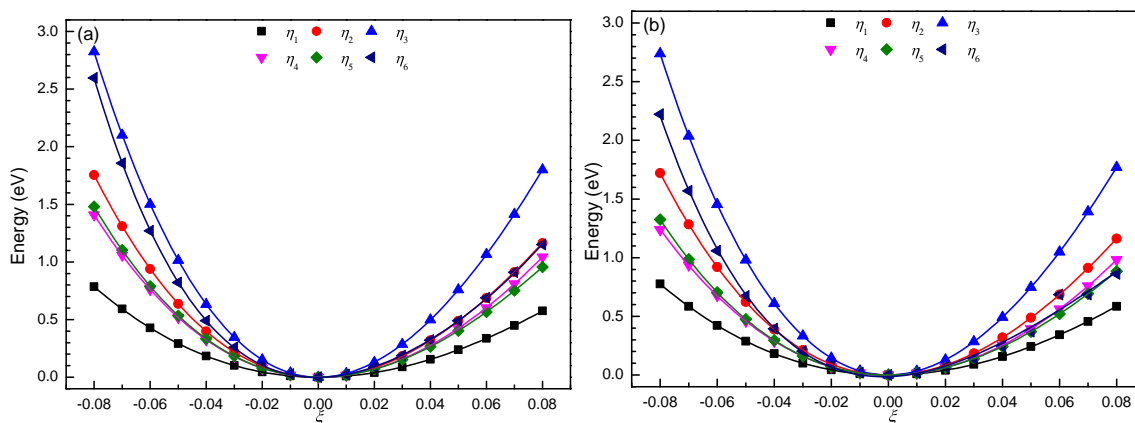


Figure 1. The strain–energy relations for (a) LaB₆ and (b) CeB₆. The discrete points and the solid lines represent the density functional theory (DFT) results and the results of third-order polynomial fitting, respectively.

The TOECs allow the determination of anharmonic properties of crystals, such as thermal expansion, interactions of acoustic and thermal phonons, and temperature and pressure dependence of elastic constants. The evaluation of the TOECs is of general interest. The calculated TOECs of LaB₆ and CeB₆ are given in Table 3. All the TOECs of the two hexaborides are negative except for the values of C_{123} (=254.3 GPa (304.8 GPa) for LaB₆ (CeB₆)). The absolute values of their longitudinal mode C_{111} (=−2647.1 GPa (−2568.4 GPa) for LaB₆ (CeB₆)) were found to be much greater than the corresponding shear modes C_{112} , C_{123} , C_{144} , C_{155} , and C_{456} , implying the contribution to lattice

vibrations from their longitudinal modes is much greater. The highest absolute values of C_{111} indicate a pronounced anisotropy in both materials. Unfortunately, no measurements or calculations on the TOECs of LaB_6 and CeB_6 are available for comparison.

Table 3. Third-order elastic constants C_{ijk} (in GPa) of LaB_6 and CeB_6 .

Crystal	C_{111}	C_{112}	C_{123}	C_{144}	C_{155}	C_{456}
LaB_6	−2647.1	−373.2	254.3	−167.6	−340.4	−403.8
CeB_6	−2568.4	−402.8	304.8	−69.6	−286.9	−408.4

3.2. Pressure Derivatives of the Effective Second-Order Elastic Constants of REB_6 ($\text{RE} = \text{La}, \text{Ce}$)

The TOECs above were further used to evaluate the first-order pressure derivatives of LaB_6 and CeB_6 . These values are summarized in Table 4. A linear increase with pressure was observed for C_{11} , C_{12} , C_{44} with pressure derivative C'_{ij} of 4.586, 1.895, 0.451 and 4.507, 1.921, 0.085 for LaB_6 and CeB_6 . The pressure-induced variation in the longitudinal mode C_{11} was the largest, followed by the shear mode C_{12} , and the smallest for the pure shear mode C_{44} . For the two hexaborides, the effect of the pressure on the C_{12} was obviously smaller than that on the C_{11} , but markedly greater than that on the C_{44} . Under hydrostatic pressure, the Born stability criteria for the cubic system are given by [9]

$$\begin{aligned} K_1 &= \tilde{C}_{11}^P + 2\tilde{C}_{12}^P > 0, \\ K_2 &= \tilde{C}_{11}^P - \tilde{C}_{12}^P > 0, \\ K_3 &= \tilde{C}_{44}^P > 0, \end{aligned} \quad (15)$$

with

$$\begin{aligned} \tilde{C}_{ii}^P &= C_{ii}(P) - P (i = 1, 4), \\ \tilde{C}_{12}^P &= C_{12}(P) + P. \end{aligned} \quad (16)$$

In terms of the effective SOECs, these criteria can be expressed as

$$\begin{aligned} K_1 &= (C_{11} + 2C_{12}) + (C'_{11} + 2C'_{12} + 1)P > 0, \\ K_2 &= (C_{11} - C_{12}) + (C'_{11} - C'_{12} - 2)P > 0, \\ K_3 &= C_{44} + (C'_{44} - 1)P > 0. \end{aligned} \quad (17)$$

From the pressure derivatives of the SOECs, the first-order pressure derivatives of K_1 and K_2 were calculated as 9.376 (9.349) and 0.691 (0.586) for LaB_6 (CeB_6), while that of the corresponding K_3 was calculated to be −0.549 (−0.915). Thus, the K_1 and K_2 values of both materials linearly increase while the K_3 values linearly decrease with increasing pressure. When the pressure applied to LaB_6 (CeB_6) is beyond 164.1 GPa (81.7 GPa), the K_3 has a negative value, as shown in Figure 2. This indicates that the cubic structure of LaB_6 (CeB_6) can remain mechanically stable up to 164.1 GPa (81.7 GPa). Previous high-pressure phase transitions showed that no structural phase transitions occur up to 25 GPa (85 GPa) for LaB_6 (CeB_6) [11–13]. Therefore, the results of the present work are basically consistent with those of previous experiments.

Table 4. Pressure derivatives C'_{ij} of the second-order elastic constants of LaB_6 and CeB_6 .

Crystal	C'_{11}	C'_{12}	C'_{44}
LaB_6	4.586	1.895	0.451
CeB_6	4.507	1.921	0.085

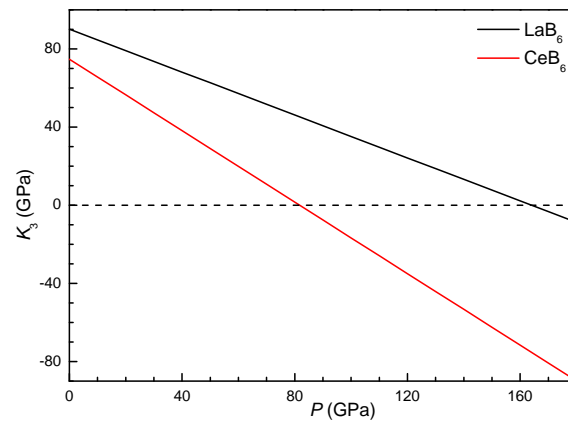


Figure 2. The pressure dependence of the K_3 values of LaB_6 and CeB_6 .

3.3. Pressure Derivatives of the Polycrystalline elastic moduli of REB_6 ($\text{RE} = \text{La}, \text{Ce}$)

The polycrystalline bulk (B), shear (G), and Young's (E) moduli and Poisson's ratio (ν) of LaB_6 and CeB_6 were calculated based on their single crystal SOECs, which are collected in Table 5. The calculated bulk modulus (174.2 GPa) of LaB_6 agrees well with the reported experimental values of 163, 184, 188, 164 ± 2 , 173 ± 7 , and 172 GPa [2–4,11,37], and the previous theoretical results of 185 and 180 GPa [3,8]. For CeB_6 , the calculated bulk modulus (174.7 GPa) of the present study are also in good accordance with experimental measurements of 191, 168, 182, and 166 GPa [5,7,12] and other theoretical results of 173 and 166.8 GPa [8,9]. The calculated G value of 120.9 GPa is excellently consistent with that of 121.2 GPa reported in Ref. [9]. The pressure derivatives of the bulk modulus and shear modulus of the two hexaborides are calculated using the pressure derivatives of the single crystal SOECs, and then those of the Young's modulus and the Poisson's ratio are also estimated. All the obtained results are presented in Table 6. The calculated B' value of 2.792 (2.783) for LaB_6 (CeB_6) can compare well with the experimental value of 4.2 ± 1.5 [11] (3.15 [12]). One can see that the B' and G' are positive for both materials, which agree well with the corresponding C'_{ij} s. A similar behavior is found for the E' and ν' being positive, and is in good accordance with the B' and G' . The bulk modulus is a measure of the resistance of a material to volume changes. The shear modulus is a measure of the resistance of a material to shear deformation. The bulk modulus and shear modulus play an important role in determining the strength of solids [38]. Usually, a superhard material has a high bulk modulus, high shear modulus, and high shear strength. Thus, we can predict that LaB_6 and CeB_6 have high hardness. The positive values of B' and G' mean that the elastic moduli B and G can increase gradually with the pressure, showing that the two hexaborides with a simple cubic structure became more difficult to compress and shear as the pressure increased. The Young's modulus is a measure of the stiffness of a material. The larger the value of E , the stiffer the material. The positive values of E' demonstrate that LaB_6 and CeB_6 become more and more stiff as the pressure increases.

Table 5. Polycrystalline bulk modulus B , shear modulus G , and Young's modulus E (in GPa), and Poisson's ratio ν of LaB_6 and CeB_6 .

Crystal	Method	B	G	E	ν	B/G
LaB_6	Voigt	174.2	144.0	338.8	0.176	
	Reuss	174.2	118.5	289.8	0.223	
	Hill	174.2	131.3	314.8	0.199	1.327
CeB_6	Voigt	174.7	138.9	329.4	0.186	
	Reuss	174.7	102.8	257.8	0.254	
	Hill	174.7	120.9	294.6	0.219	1.445

Table 6. Pressure derivatives of polycrystalline elastic modulus B' (bulk modulus), G' (shear modulus), and E' (Young's modulus), and Poisson's ratio ν' of LaB_6 and CeB_6 .

Crystal	Method	B'	G'	E'	$\nu'(\times 10^{-3})$	$(B/G)'$
LaB_6	Voigt	2.792	0.809	2.664	2.645	0.014
	Reuss	2.792	0.618	2.089	2.445	
	Hill	2.792	0.713	2.379	2.550	
CeB_6	Voigt	2.783	0.568	2.165	2.942	0.018
	Reuss	2.783	0.196	1.084	2.886	
	Hill	2.783	0.382	1.636	2.918	

Pugh [39] has introduced the ratio between the bulk modulus and the shear modulus (B/G) to assess the ductile/brittle behaviors of a material. A high (low) B/G value is correlated with the ductility (brittleness) of the material. The critical value of the brittle-to-ductile transition was observed to be ~ 1.75 . The B/G ratio was calculated as 1.327 (1.445) for LaB_6 (CeB_6) at ground-state, indicating the brittleness of the hexaboride. The pressure derivative $(B/G)'$ can be obtained from those of the bulk modulus and the shear modulus, which is expressed as $(B/G)' = (B'G - BG')/G^2$. On this basis, the $(B/G)'$ value was evaluated to be 0.014 (0.018) for LaB_6 (CeB_6), showing that the B/G ratio can increase with increasing pressure. The pressure at which a brittle-to-ductile transition happens is predicted as 30.1 GPa (16.5 GPa) for LaB_6 (CeB_6). Frantsevich et al. [40] distinguished the ductility/brittleness of the materials in terms of Poisson's ratio. Generally, a brittle material has a lower Poisson's ratio than 0.26. The ground-state value of the Poisson's ratio is consistent with the B/G ratio for LaB_6 (CeB_6). The very small and positive values of ν' imply a very slow increase of the ν of both materials with the pressure. Pettifor [41] introduced the Cauchy pressure to describe the covalent character of atomic bonding related to the ductile/brittle characteristics of a material. He suggested that larger positive Cauchy pressure corresponds to a ductile material with more metallic bonds, whereas larger negative values indicate a brittle behavior with a more covalent character of bonds. For a cubic system, the Cauchy pressure P_c is defined as $P_c = C_{12} - C_{44}$. The P_c of LaB_6 (CeB_6) was calculated as -65.9 GPa (-58.6 GPa) in terms of the ground-state SOECs given in Table 2. We can find that the bonding of both materials is covalent with $B/G < 1.75$, leading to a brittle behavior. The pressure derivative P'_c can be obtained from those of the effective SOECs, which is given by $P'_c = C'_{12} - C'_{44}$. The P'_c value of LaB_6 (CeB_6) was estimated to be 1.444 (1.836) based on the values of C'_{12} and C'_{44} given in Table 4, showing the increase of the Cauchy pressure with the pressure. Overall, the brittleness of LaB_6 (CeB_6) can reduce as the pressure increases, which is consistent with the previous theoretical result [9].

3.4. Pressure Derivatives of the Elastic Anisotropy of REB_6 ($\text{RE} = \text{La}, \text{Ce}$)

The elastic anisotropy of a material has an important implication in engineering science due to its high association with the possibility of inducing microcracks in the material [42]. The elastic anisotropy factor for a cubic crystal introduced firstly by Zener [43] is expressed as

$$A_Z = \frac{2C_{44}}{(C_{11} - C_{12})}. \quad (18)$$

A single crystal with $A_Z = 1$ is isotropic, while values smaller or greater than unity describe the degree of elastic anisotropy. The pressure derivative A'_Z can be obtained from those of the effective SOECs, which is given by

$$A'_Z = \frac{[C'_{44}(C_{11} - C_{12}) - C_{44}(C'_{11} - C'_{12})]}{(C_{11} - C_{12})^2}. \quad (19)$$

Subsequently, Chung and Buessem [44] empirically improved the anisotropy factor of Zener by

$$A_C = \frac{(G_V - G_R)}{(G_V + G_R)}. \quad (20)$$

A single crystal with $A_C = 0$ is isotropic, otherwise it is anisotropic. The pressure derivative A'_C can be obtained from those of the elastic modulus G'_V and G'_R , which is given by

$$A'_C = \frac{2(G'_V G_R - G_V G'_R)}{(G_V + G_R)^2}. \quad (21)$$

However, it is noteworthy that A_Z and A_C do not account for the bulk part of the elastic stiffness tensor, and they are only effective for cubic crystals. To consider the contributions of the shear modulus and bulk modulus, Shivakumar et al. [45] proposed a universal anisotropy index that is applicable to various crystal systems, which was expressed as $A_S = B_V/B_R + 5G_V/G_R - 6$. A nonzero value of A_S is a measure of the anisotropy. Because the B_V is equal to the B_R for cubic system, the A_S can be simplified as

$$A_S = 5\left(\frac{G_V}{G_R} - 1\right). \quad (22)$$

The pressure derivative A'_S can be calculated in terms of those of the elastic modulus G'_V and G'_R , which is given by

$$A'_S = 5\frac{(G'_V G_R - G_V G'_R)}{G_R^2}. \quad (23)$$

In terms of the SOECs, the elastic moduli, and the corresponding pressure derivatives above, we predicted the values and the pressure derivatives of various anisotropy factors for LaB_6 and CeB_6 , as presented in Table 7. The A_Z values of less than one and the nonzero A_C and A_S values show the elastic anisotropy of the two hexaborides at ground-state. Meanwhile, the negative values of A'_Z and the positive ones of A'_C and A'_S values indicate that the corresponding anisotropy factors can be far away from unity with increasing pressure. These results show that the anisotropy of both materials can be enhanced by increasing the pressure.

Table 7. Anisotropic factors A of LaB_6 and CeB_6 and their pressure derivatives A' ($\times 10^{-4}$).

Crystal	A_Z	A'_Z	A_C	A'_C	A_S	A'_S
LaB_6	0.401	−1.956	0.097	2.002	1.076	24.560
CeB_6	0.318	−6.900	0.149	10.700	1.756	147.830

4. Conclusions

The SOECs and TOECs of rare-earth hexaborides LaB_6 and CeB_6 have been determined by using first-principles calculations and homogeneous deformation methods. The calculated lattice parameters, SOECs, and bulk moduli are in reasonable accordance with the available experimental and theoretical values. All the TOECs of both hexaborides have negative values except for C_{123} . The highest absolute values of the longitudinal modes C_{111} show that their contribution to lattice vibrations is the greatest, and so also their anisotropy in C_{111} . From the calculated elastic constants, the pressure derivatives of the effective SOECs have been investigated along with the pressure effects on the structural stability, mechanical properties, and elastic anisotropy. As the pressure increases, the mechanical stability reduces, and the ductility and anisotropy increase for both hexaborides. The full set of TOECs of both materials have been determined for the first time, and comparison could not be made as the same is not available in literature. The measurements of the TOECs are essential for the research of LaB_6 and CeB_6 in the future.

Acknowledgments: The work is supported by the Natural Science Foundation of China (51661013, 51461020, 11464020) and the Ph.D. Start-up Fund of Natural Science Foundation of Jinggangshan University (JZB15007).

Author Contributions: X.Z. and Y.W. conceived and designed the calculations; Y.Y. and Q.G. performed the calculations; P.O. checked the data; X.Z., S.Z. and Y.W. analyzed the data; X.Z. wrote the paper.

Conflicts of Interest: The authors declare no conflict of interest.

References

1. Ji, X.H.; Zhang, Q.Y.; Xu, J.Q.; Zhao, Y.M. Rare-earth hexaborides nanostructures Recent advances in materials, characterization and investigations of physical properties. *Prog. Solid State Chem.* **2011**, *39*, 51–69.
2. Tanaka, T.; Yoshimoto, J.; Ishli, M.; Bannai, E.; Kawai, S. Elastic constants of LaB₆ at room temperature. *Solid State Commun.* **1977**, *22*, 203–205.
3. Baranovskiy, A.; Grechnev, G.; Fil, V.; Ignatova, T.; Logosha, A.; Panfilov, A.; Svechkarev, I.; Shitsevalova, N.; Filippov, V.; Eriksson, O. Electronic structure, bulk and magnetic properties of MB₆ and MB₁₂ borides. *J. Alloys Compd.* **2007**, *442*, 228–230.
4. Nakamura, S.; Goto, T.; Kasaya, M.; Kunii, S. Electron-strain interaction in valence fluctuation compound SmB₆. *J. Phys. Soc. Jpn.* **1991**, *60*, 4311–4318.
5. Nakamura, S.; Goto, T.; Kunii, S.; Iwashita, K.; Tamaki, A. Quadrupole-strain interaction in rare-earth hexaborides. *J. Phys. Soc. Jpn.* **1994**, *63*, 623–636.
6. Goto, T.; Tamaki, A.; Kunii, S.; Nakajima, T.; Fujimura, T.; Kasuya, T.; Komatsubara, T.; Woods, S.B. Elastic properties in CeB₆. *J. Magn. Magn. Mater.* **1983**, *31–34*, 419–420.
7. Lüthi, B.; Blumenröder, S.; Hillebrands, B.; Zirngiebl, E.; Güntherodt, G.; Winzer, K. Elastic and magnetoelastic effects in CeB₆. *J. Magn. Magn. Mater.* **1985**, *58*, 321–322.
8. Gürel, T.; Eryiğithys, R. *Ab initio* lattice dynamics and thermodynamics of rare-earth hexaborides LaB₆ and CeB₆. *Phys. Rev. B* **2010**, *82*, 104302–104313.
9. Tang, M.; Liu, L.; Cheng, Y.; Ji, G.J. First-principles study of structural, elastic, and electronic properties of CeB₆ under pressure. *Front. Phys.* **2015**, *10*, 107104–107109.
10. Teredesai, P.; Muthu, D.V.S.; Chandrabhas, N.; Meenakshi, S.; Vijayakumar, V.; Modak, P.; Rao, R.S.; Godwal, B.K.; Sikka, S.K.; Sood, A.K. High pressure phase transition in metallic LaB₆: Raman and X-ray diffraction studies. *Solid State Commun.* **2004**, *129*, 791–796.
11. Godwal, B.K.; Petruska, E.A.; Speziale, S.; Yan, J.; Clark, S.M.; Kruger, M.B.; Jeanloz, R. High-pressure Raman and X-ray diffraction studies on LaB₆. *Phys. Rev. B* **2009**, *80*, 172104–172107.
12. Leger, J.M.; Rossat-Mignod, J.; Kunii, S.; Kasuya, T. High pressure compression of CeB₆. *Solid State Commun.* **1985**, *54*, 995–997.
13. Foroozani, N.; Lim, J.; Fabbris, G.; Rosa, P.F.S.; Fisk, Z.; Schilling, J.S. Suppression of dense Kondo state in CeB₆ under pressure. *Physica B* **2015**, *457*, 12–16.
14. Zhao, J.J.; Winey, J.M.; Gupta, Y.M. First-principles calculations of second- and third-order elastic constants for single crystals of arbitrary symmetry. *Phys. Rev. B* **2007**, *75*, 94105–94111.
15. Łopuszyński, M.; Majewski, J.A. *Ab initio* calculations of third-order elastic constants and related properties for selected semiconductors. *Phys. Rev. B* **2007**, *76*, 45202–45209.
16. Wang, H.; Li, M. *Ab initio* calculations of second-, third-, and fourth-order elastic constants for single crystals. *Phys. Rev. B* **2009**, *79*, 224102–224111.
17. Kresse, G.; Hafner, J. *Ab initio* molecular dynamics for open-shell transition metals. *Phys. Rev. B* **1993**, *48*, 13115–13118.
18. Kresse, G.; Furthmüller, J. Efficiency of *ab-initio* total energy calculations for metals and semiconductors using a plane-wave basis set. *Comput. Mater. Sci.* **1996**, *6*, 15–50.
19. Kresse, G.; Furthmüller, J. Efficient iterative schemes for *ab initio* total-energy calculations using a plane-wave basis set. *Phys. Rev. B* **1996**, *54*, 11169–11186.
20. Blöchl, P.E. Projector augmented-wave method. *Phys. Rev. B* **1994**, *50*, 17953–17979.
21. Kresse, G.; Joubert, D. From ultrasoft pseudopotentials to the projector augmented-wave method. *Phys. Rev. B* **1999**, *59*, 1758–1775.
22. Perdew, J.P.; Burke, K.; Ernzerhof, M. Generalized gradient approximation made simple. *Phys. Rev. Lett.* **1996**, *77*, 3865–3868.

23. Perdew, J.P.; Burke, K.; Ernzerhof, M. Generalized gradient approximation made simple [Phys. Rev. Lett. 77, 3865 (1996)]. *Phys. Rev. Lett.* **1997**, *78*, 1396.
24. Monkhorst, H.J.; Pack, J.D. Special points for Brillouin-zone integrations. *Phys. Rev. B* **1976**, *13*, 5188–5192.
25. Birch, F. Finite elastic strain of cubic crystals. *Phys. Rev.* **1947**, *71*, 809–824.
26. Thurston, R.; Brugger, K. Third-order elastic constants and the velocity of small amplitude elastic waves in homogeneously stressed media. *Phys. Rev.* **1964**, *135*, 3.
27. Brugger, K. Thermodynamic definition of higher order elastic coefficients. *Phys. Rev.* **1964**, *133*, 1611–1612.
28. Hiki, Y. High-order elastic constants of solids. *Annu. Rev. Mater. Sci.* **1981**, *11*, 51–73.
29. Rao, R.R.; Padmaja, A. Effective second-order elastic constants of a strained crystal using the finite strain elasticity theory. *J. Appl. Phys.* **1987**, *62*, 440–443.
30. Voigt, W. *Lehrbuch der Kristallphysik*; Taubner: Leipzig, Germany, 1928.
31. Reuss, A. Calculation of the flow limits of mixed crystals on the basis of the plasticity of monocrystals. *Z. Angew. Math. Mech.* **1929**, *9*, 49–58.
32. Hill, R. The elastic behaviour of a crystalline aggregate. *Proc. Phys. Soc. A* **1952**, *65*, 349–354.
33. Chen, C.H.; Aizawa, T.; Iyi, N.; Sato, A.; Otani, S. Structural refinement and thermal expansion of hexaborides. *J. Alloys Compd.* **2004**, *366*, L6–L8.
34. Tanaka, K.; Ōnuki, Y. Observation of 4f electron transfer from Ce to B₆ in the Kondo crystal CeB₆ and its mechanism by multitemperature X-ray diffraction. *Acta Cryst. B* **2002**, *58*, 423–436.
35. Clementi, E.; Raimondi, D.L.; Reinhardt, W.P. Atomic screening constants from SCF functions. II. Atoms with 37 to 86 Electrons. *J. Chem. Phys.* **1967**, *47*, 1300–1307.
36. Mouhat, F.; Coudert, F.X. Necessary and sufficient elastic stability conditions in various crystal systems. *Phys. Rev. B* **2014**, *90*, 224104–224107.
37. Lundström, T.; Lönnberg, B.; Törmä, B.; Etourneau, J.; Tarascon, J.M. An investigation of the compressibility of LaB₆ and EuB₆ using a high pressure X-ray power diffraction technique. *Phys. Scr.* **1982**, *26*, 414–416.
38. Teter, D.M. Computational alchemy: The search for new superhard materials. *MRS Bull.* **1998**, *23*, 22–27.
39. Pugh, S.F. Relations between the elastic moduli and the plastic properties of polycrystalline pure metals. *Philos. Mag.* **1954**, *45*, 823–843.
40. Frantsevich, I.N.; Voronov, F.F.; Bokuta, S.A. In *Elastic Constants and Elastic Moduli of Metals and Insulators Handbook*; Frantsevich, I.N., Ed.; Naukova Dumka: Kiev, Ukraine, 1983; pp. 60–180.
41. Pettifor, D.G. Theoretical predictions of structure and related properties of intermetallics. *Mater. Sci. Technol.* **1992**, *8*, 345–349.
42. Tvergaard, V.; Hutchinson, J.W. Microcracking in ceramics induced by thermal expansion or elastic anisotropy. *J. Am. Ceram. Soc.* **1988**, *71*, 157–166.
43. Zener, C. *Elasticity and Anelasticity of Metals*; University of Chicago: Chicago, IL, USA, 1984.
44. Chung, D.H.; Buessem, W.R. The elastic anisotropy of crystals. *J. Appl. Phys.* **1967**, *38*, 2010–2012.
45. Ranganathan, S.I.; Ostoja-Starzewski, M. Universal elastic anisotropy index. *Phys. Rev. Lett.* **2008**, *101*, 55504–55507.

